Removal of Inclusions from Molten Aluminum by Supergravity Filtration

GAOYANG SONG, BO SONG, ZHANBING YANG, YUHOU YANG, and JING ZHANG

A new approach to removing inclusions from aluminum melt by supergravity filtration was investigated. The molten aluminum containing $MgAl_2O_4$ spinel and coarse Al_3Ti particles was isothermally filtered with different gravity coefficients, different filtering times, and various filtering temperatures under supergravity field. When the gravity coefficient $G \geq 50$, the alloy samples were divided automatically into two parts: the upper residue and the lower filtered aluminum. All inclusions ($MgAl_2O_4$ and Al_3Ti particles) were nearly intercepted in the upper residue by filter felt with average pore size of 44.78 μm. The removal efficiencies of oxide inclusions and Al_3Ti particles exceeded 98 and 90 pct, respectively, at $G \geq 50$, $t = 2$ minutes, $T = 973$ K (700 °C). Besides, the yield of purified aluminum was up to 92.1 pct at $G = 600$, $t = 2$ minutes, and $T = 973$ K (700 °C). The calculations of centrifugal pressure indicated that supergravity filtration could effectively overcome the pressure drop without meeting the rigorous requirement of height of molten metal, especially for using the fine-pore filter medium. Moreover, cake-mode filtration was the major mechanism of supergravity filtration of molten metal in this work.

DOI: 10.1007/s11663-016-0775-x

I. INTRODUCTION

A typical molten aluminum generally contains a large number of contaminants, such as nonmetallic inclusions (especially oxides, nitrides, and carbides), intermetallic compounds (such as iron-rich phase), and dissolved gasses (especially hydrogen), during the processes of smelting and refining.[1] The presence of these contaminants, such as nonmetallic inclusions, is considered to have detrimental effects on the castability,[2] machinability,[3] and mechanical properties[4] of alloys. The increasing desire for high-quality aluminum alloys to be used in the automobile manufacturing and aerospace industry, as well as for construction and electrical components,[5] has strongly motivated manufacturers to produce cleaner aluminum alloys. Therefore, further reducing the level of inclusions from aluminum melt is necessary with respect to the metal yield and quality.

Removal of inclusions from liquid aluminum alloys is an essential melt treatment step in the refining process. Many different conventional methods have been applied for removing inclusions from aluminum melt, such as sedimentation,[6] filtration,[5,7] bubble floatation,[8] and flux refining.[9] However, these methods can hardly meet the cleanliness level requirement in many applications because of their low removal efficiency in the case of very fine size and small difference in density between inclusion and metal.[6,10] Therefore, innovative or improved methods for removing inclusion deserve to be explored.

In recent years, the supergravity method has attracted much attention due to its efficiency in removing the inclusions and its higher yield.[11] Supergravity technology has been studied to remove the impurity elements (such as Fe and Si) from aluminum alloys[12,13] and to purify metallurgical grade silicon,[14] as well as to enrich the valuable elements (such as Ti, V, and RE) from various metallurgical slags,[15–17] and has been proven to be a potential high-efficiency separation method. However, the study on separating nonmetallic inclusions from the aluminum melt with supergravity is seldom reported as a whole. Separation behavior of nonmetallic inclusions ($MgAl_2O_4$ spinel) in aluminum melt with supergravity has been investigated in our earlier study,[18] which indicated that supergravity separating technology for purifying metal melt is an effective method. However, it is noteworthy that inclusions were just gathered to the bottom area of samples and not separated from aluminum matrix thoroughly. Also, further treatment is required to separate these inclusions using mechanical and chemical methods. Therefore, it is essential to develop a new method to separate inclusions effectively from molten aluminum under supergravity field without any effort for further separation.

In this work, separating the contaminants (especially nonmetallic inclusions) from aluminum melt through filtration combined with supergravity was explored. Simultaneously, the effects of the gravity coefficient, filtering time, and filtering temperature on the removal of inclusions from aluminum melt have also been

GAOYANG SONG, YUHOU YANG, and JING ZHANG, Ph.D. Candidates, BO SONG, Professor, and ZHANBING YANG, Associate Professor, are with the School of Metallurgical and Ecological Engineering and the State Key Laboratory of Advanced Metallurgy, University of Science and Technology Beijing, Beijing 100083, China. Contact email: songbo@metall.ustb.edu.cn
Manuscript submitted April 25, 2016.
Article published online September 20, 2016.

investigated. Besides, the centrifugal pressure generated by supergravity was calculated and the mechanism of supergravity filtration was also discussed in this study.

II. EXPERIMENTAL

The supergravity field can be generated by a centrifugal apparatus whose schematic diagram in the working status is illustrated in Figure 1. It mainly consists of a resistance-heated furnace and a counterweight fixed symmetrically onto the horizontal rotor. The

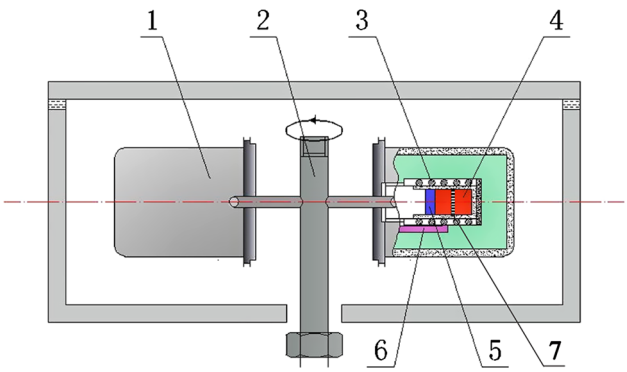

Fig. 1—Schematic view of the experimental apparatus in the working state: 1. counterweight, 2. centrifugal axis, 3. resistance coil, 4. aluminum melt, 5. covering slag, 6. thermocouple, and 7. filter.

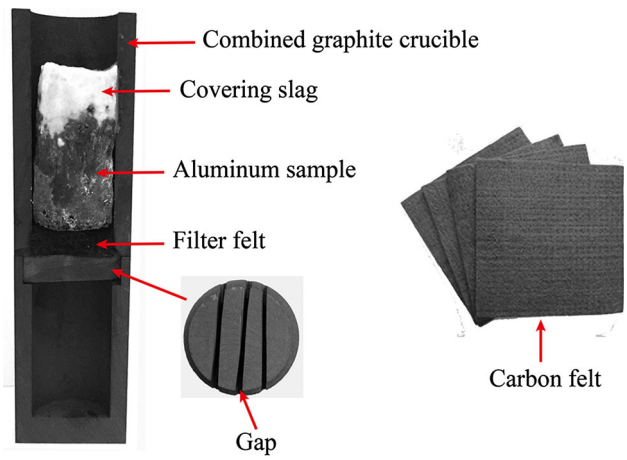

Fig. 2—Photographs of filter crucible and carbon felt.

experimental temperature can be controlled by a temperature controller within the precision range of ±3 K (±3 °C) with an R-type thermocouple. The filter unit is a self-design filter crucible, which consists of a combined graphite crucible with upper and lower containers and a filter felt embed at the bottom of the upper container, as shown in Figure 2. Generally, the most frequently used filter media in the aluminum filtration process is ceramic foam filters (CFFs).[5] However, it is difficult to tightly assemble the CFFs in the container without any gaps due to the rigid contact between them. In this case, obvious errors may be introduced into the experimental results under the supergravity field. In this work, the soft carbon felt was selected as the filter medium for separating inclusions that can solve the assembling problem, and the specifications of carbon felt are represented in Table I. In addition, the average pore size (44.78 μm) of the carbon felt used here is much smaller than that of the CFFs (window diameter more than 300 μm) investigated in many publications.[1,5,19]

The gravity coefficient was calculated as the ratio of supergravitational acceleration to normal-gravitational acceleration *via* Eq. [1]:[15]

$$G = \frac{\sqrt{g^2 + (r\omega^2)^2}}{g} = \frac{\sqrt{g^2 + \left(\frac{N^2\pi^2 r}{900}\right)^2}}{g} \qquad [1]$$

where G is the gravity coefficient, ω is the angular velocity (rad/s), N is the rotating speed (r/min), r is the distance from the centrifugal axis to the center of the sample (0.25 m); and g is the normal-gravitational acceleration (9.81 m/s^2). Here, when $N = 0$ r/min, $G = 1$; when $N > 0$ r/min, substituting $r = 0.25$ m, $\pi = 3.14$, and $g = 9.81$ m/s^2 into Eq. [1], the gravity coefficient can be approximately expressed as

$$G = 2.79 \times 10^{-4} N^2 \qquad [2]$$

The experimental aluminum alloy containing $MgAl_2O_4$ spinel inclusion (0.91 wt pct) and impurity element of Ti (2.174 wt pct) was heated to melt in a graphite crucible and poured into alloy ingots used for separating experiments. The chemical composition of the experimental alloy is represented in Table II. During the experimental process, the aluminum melt was protected from oxidation by the covering slag, which was a mixture of 33 wt pct sodium chloride and 67 wt pct calcium chloride, and both were analytical reagents.

Table I. Physical Parameters of Carbon Felt Used as Filter Medium

Average Pore Diameter (μm)	Bulk Density (g/cm^3)	Carbon Content (pct)	Thermal Conductivity (W/m K)
44.78	0.12 to 0.14	≥99.90	0.08 to 0.14

Table II. Chemical Composition of the Aluminum Alloy (Mass Pct)

Si	Mg	Fe	Cu	Ti	Sr	Cr	O	Al
7.680	1.022	0.230	0.029	2.174	0.042	0.009	0.410	bal

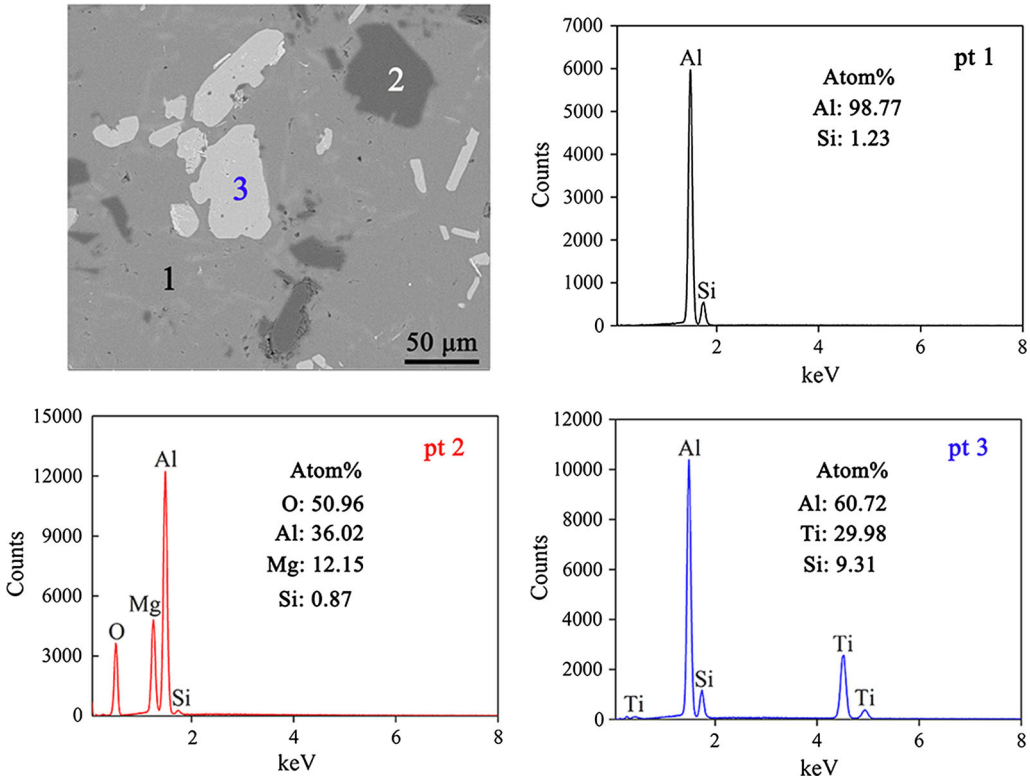

Fig. 3—Morphology and composition (at. pct) of inclusions observed by SEM-EDS.

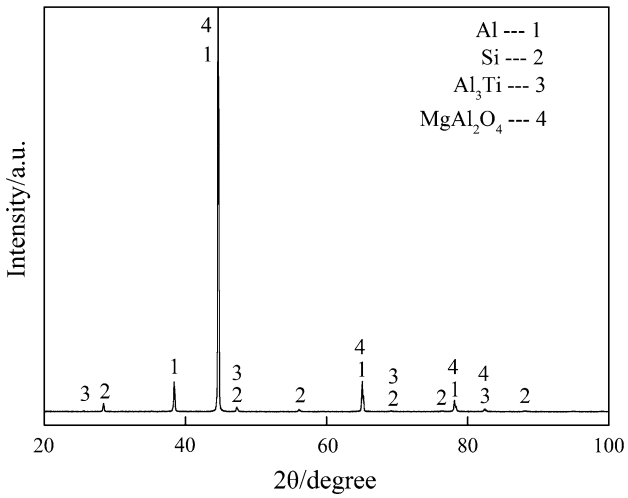

Fig. 4—X-ray diffraction pattern of the experimental alloy.

The experimental alloy (average 7 g) and the covering slag (3 g) were put into an upper graphite crucible with 14-mm inner diameter, as shown in Figure 2, and heated to the target temperature for heat preservation of 5 minutes. The specific temperatures are 863 K, 893 K, 933 K, 973 K, 1023 K, and 1073 K (590 °C, 620 °C, 660 °C, 700 °C, 750 °C, and 800 °C), respectively. Then the centrifugal apparatus was turned on and adjusted to the specified angular velocity. The centrifugal apparatus was not turned off until the target time, and then the melt was rapidly cooled by water spray. Each alloy sample obtained by filtration under the supergravity field was cut into two semicircles along the axial direction. One semicircle of alloy sample and the filtering slag formed on the filter felt were burnished and polished for microscopic observation, where the morphology, chemical composition, and distribution of inclusions were investigated through an optical microscope (9XB-PC type), an X-ray diffractometer (XRD, M21X VAHF), and a scanning electron microscope-energy-dispersive spectroscope (SEM-EDS, MLA250, FEI Hong Kong Company Limited, Hong Kong, China). About 5000 inclusions ($MgAl_2O_4$ and Al_3Ti) in the experimental alloy were randomly counted by the SEM, and from those, the average size and size distribution of inclusions were measured using Image-Pro Plus™ 6.0 (Media Cybernetics, Inc., Rockville, MD). The other half of the alloy sample was used for determining the contents of O and Ti by the O and N analyzer (LECO ONH836) and the inductively coupled plasma-optical emission spectrometer (OPTIMA 7000 DV, PerkinElmer, Inc., Shanghai, China), respectively.

III. RESULTS AND DISCUSSION

A. *Observation of Inclusions in the Experimental Alloy for Supergravity Filtration*

Figures 3 and 4 show the inclusions in the experimental alloy, which can be identified as $MgAl_2O_4$ spinel particle and Al_3Ti particle by SEM-EDS and XRD. The appearance of the $MgAl_2O_4$ particle is irregular polygonal, and the shape of the Al_3Ti particle is light-gray

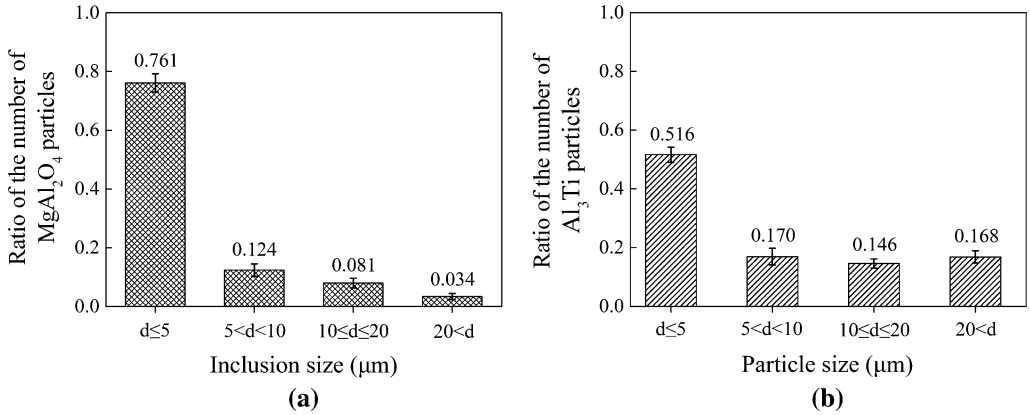

Fig. 5—Size distribution of inclusions in the experimental alloy: (*a*) $MgAl_2O_4$ particles and (*b*) Al_3Ti particles.

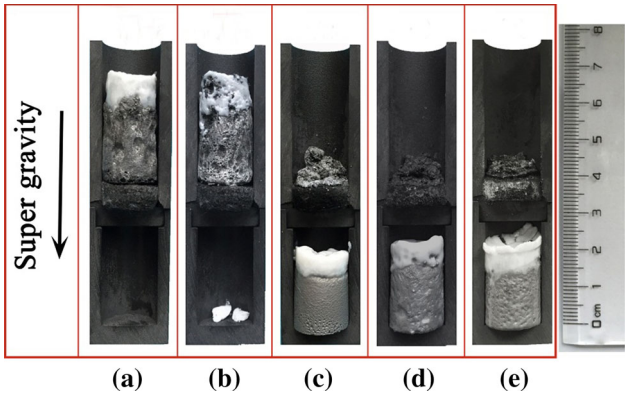

Fig. 6—Macrographs of samples obtained by filtration with different gravity coefficients: (*a*) $G = 1$, (*b*) $G = 30$, (*c*) $G = 50$, (*d*) $G = 200$, and (*e*) $G = 500$.

platelet, as shown in Figure 3. Figure 5 shows the size distribution of $MgAl_2O_4$ and Al_3Ti particles in the aluminum alloy, and the average diameters of $MgAl_2O_4$ and Al_3Ti particles are 5.43 and 9.58 μm, respectively. Generally, Ti with proper content not only acts as the dispersion-strengthening effect, but also refines grain for aluminum alloy contributing to the fine dispersed Al_3Ti particles. However, the coarse Al_3Ti particles can restrict the grain-refining effect and cause casting difficulties of aluminum melt.[20] The concentration of Ti is up to 2.17 wt pct in this experimental alloy, and there are a large number of coarse Al_3Ti particles, as seen in Figure 3. Hence, in this work, the Al_3Ti particles will be treated as a detrimental inclusion in this alloy system and will be further separated, together with the oxide inclusion ($MgAl_2O_4$), by filtration under supergravity field.

B. *Macro and Micro Observation of the Samples Obtained by Filtration under Supergravity Field*

Figure 6 shows the photographs of samples obtained by filtration with various gravity coefficients at the filtering time $t = 2$ minutes and the filtering temperature $T = 973$ K (700 °C). It is seen from Figure 6(a) that the alloy sample and covering slag are still on the filter felt within the upper crucible due to the overlarge filtration resistance from filter felt. Part of the covering slag separates to the lower container, but the alloy sample remains in the upper crucible at the gravity coefficient $G = 30$, as illustrated in Figure 6(b). When the gravity coefficient $G \geq 50$, the aluminum melt and covering slag are both separated to the lower container, leaving the upper residue on the filter felt, as shown in Figures 6(c) through (e), indicating that the large filtration resistance can be overcome by supergravity in the case of $G \geq 50$.

$MgAl_2O_4$, Al_3Ti, and Al_2O_3 particles in the upper residue obtained by filtration are observed and identified by SEM and XRD, as shown in Figure 7. As the filtration proceeds, the covering slag is separated quickly to the lower container through the filter felt, leaving the upper residue melt exposed in the atmosphere. The aluminum melt in the upper residue is oxidized, forming filmlike Al_2O_3 inclusion. Figure 8 shows SEM mappings of inclusions in the upper residue obtained at $G = 500$; it can be clearly seen that a large number of inclusions ($MgAl_2O_4$, Al_3Ti, and Al_2O_3) are gathered in the upper residue.

As shown in Figure 9(a), inclusions ($MgAl_2O_4$ and Al_3Ti particles) distribute dispersively in the parallel sample under the normal-gravity field. However, when the gravity coefficient $G \geq 50$,the alloy samples are divided into two parts: the upper residue and the lower filtered aluminum. All inclusions are nearly intercepted in the upper residue by the filter with average pore size of 44.78 μm, while it is hard to find any large inclusions in the filtered aluminum, as shown in Figures 9(b) through (i). It is observed from Figure 9 that the concentration of inclusions gathered in the upper residue increases with an increase in the gravity coefficient, due to the fact that larger supergravity imposes the sample during filtration and more aluminum melt will flow through the filter medium in the same filtering time. In addition, as the filtration proceeds, the concentration of inclusions increases, leading to the significant increase of the melt viscosity, which indicates that the residue aluminum melt hardly flows through the filter and is retained in the upper residue, as shown in Figure 9.

With much observation and analysis with SEM-EDS at higher magnification, $MgAl_2O_4$ and Al_3Ti particles are still hardly observed in the filtered aluminum,

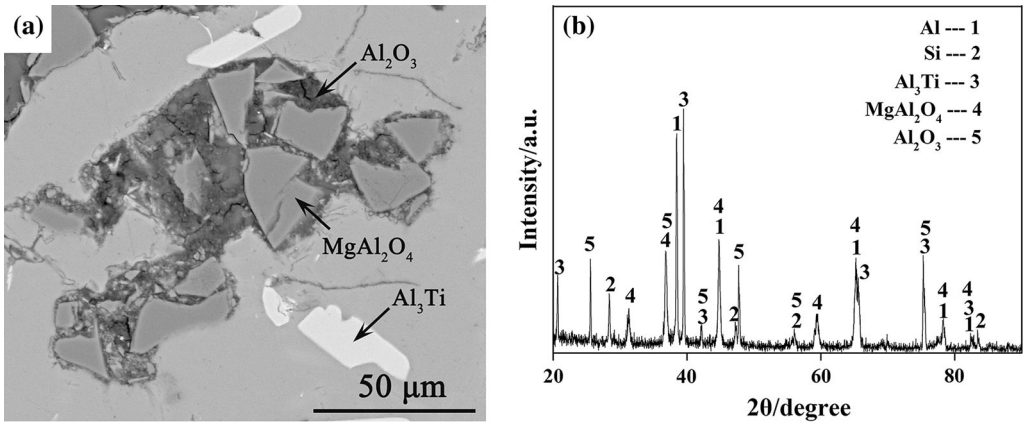

Fig. 7—Characterization of inclusions in the upper residue: (*a*) microobservation of inclusions by SEM and (*b*) XRD results of the filter residue.

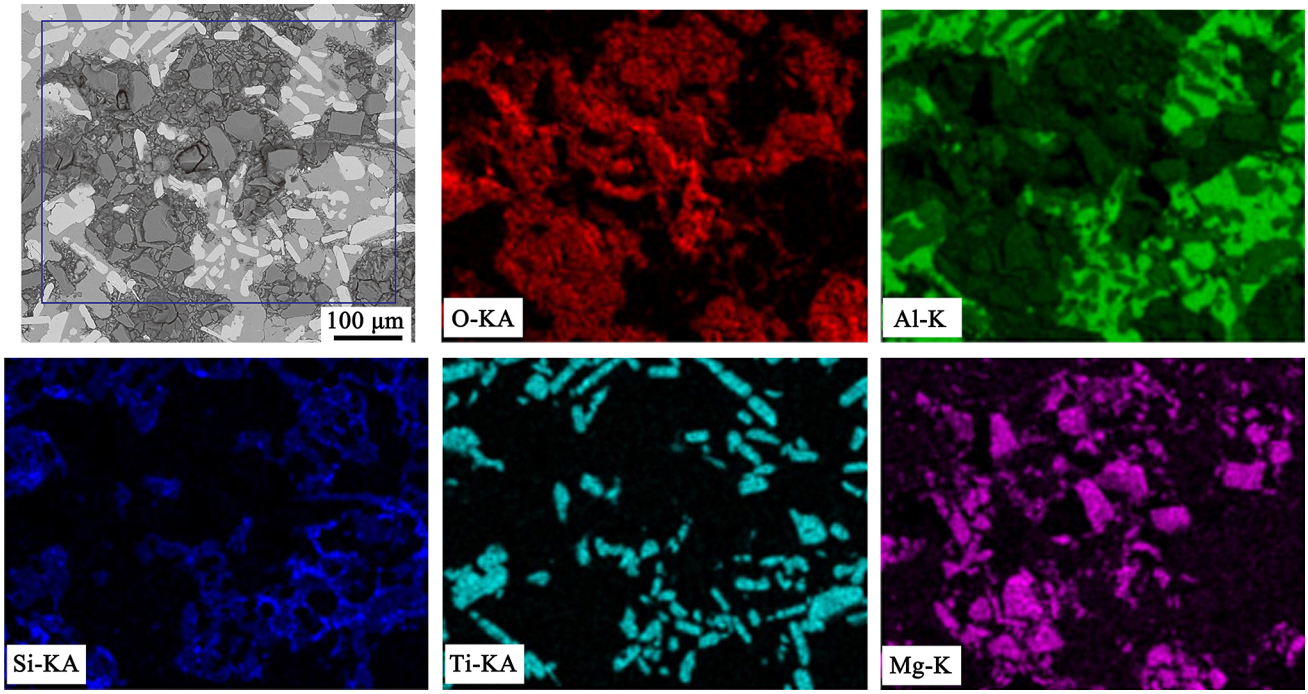

Fig. 8—SEM mapping of inclusions in the upper residue obtained at $G = 500$.

indicating that all of the inclusions in the original experimental alloy are almost removed through the supergravity filtration. However, some fine inclusions (carbon and Al_2O_3 particles) are found in the filtered aluminum, as shown in Figure 10. These fine oxide inclusions in the filtered sample may derive from the oxidation of the melt during the filtering process and pass through the filter medium with the flow of melt. Therefore, future work is required to improve the airtightness of the experimental equipment for adopting argon protection.

C. *Removal Efficiency of Inclusions and Yield of Purified Aluminum*

To evaluate the removal efficiency of inclusions (oxide inclusions and Al_3Ti particles) obtained by supergravity filtration, the contents of O and Ti in the filtered aluminum are analyzed, and the relevant results are represented in Tables III through V. The removal efficiency of inclusions is calculated *via* Eq. [3]:

$$\eta = \frac{w_0 - w_f}{w_0} \times 100\,\text{pct} \qquad [3]$$

where η is the removal efficiency of oxide inclusion or Al_3Ti inclusion and w_0 and w_f are the contents of O or Ti in the original experimental alloy and the filtered aluminum, respectively.

Due to the large filtration resistance from the fine-pore carbon felt, the aluminum melt cannot flow through the filter medium without any purifying effect under normal gravity field. When the gravity coefficient $G \geq 50$,the removal efficiencies of oxide inclusions and Al_3Ti particles exceed 98 and 90 pct, respectively, as

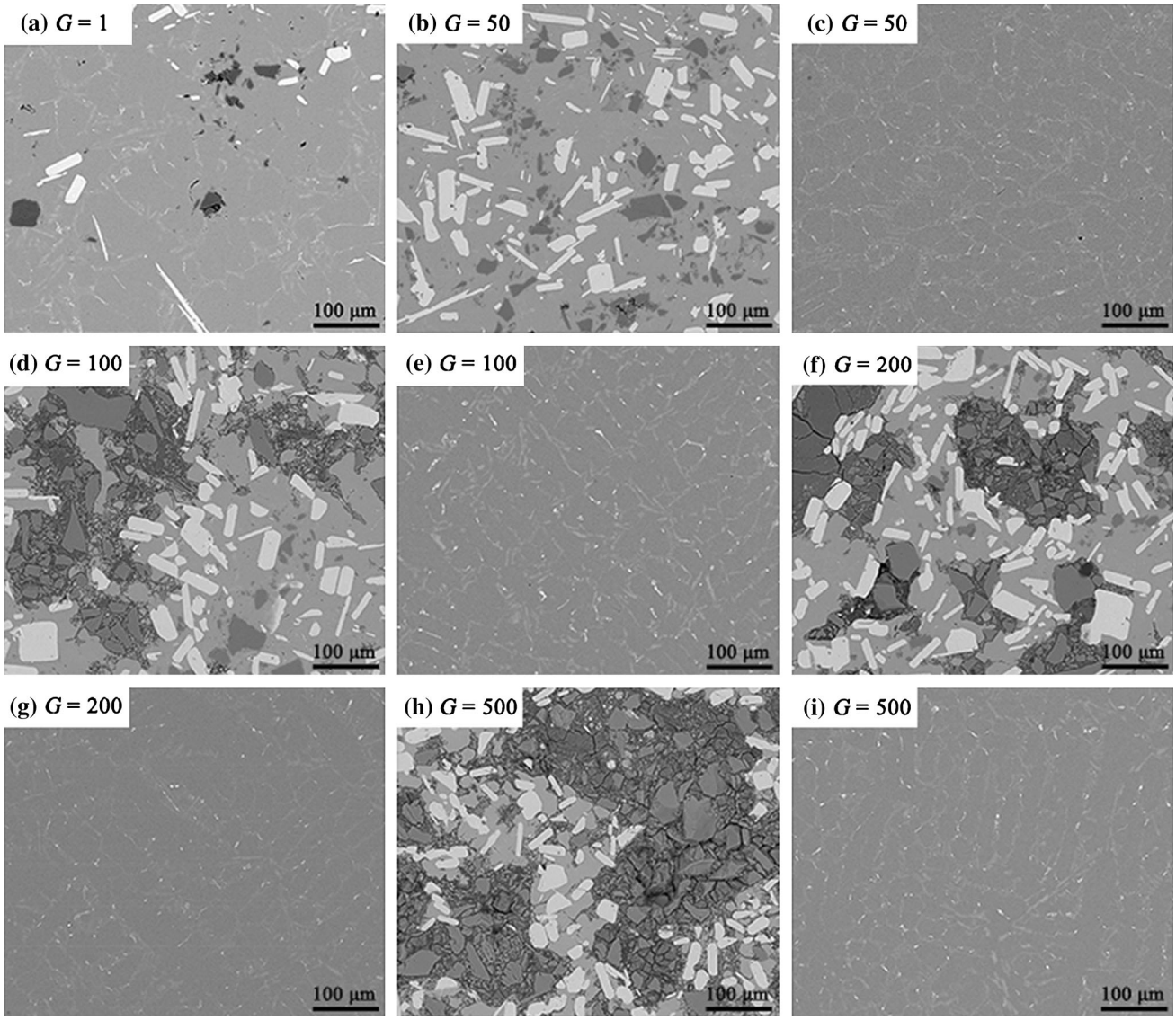

Fig. 9—Micrographs of upper residue and filtered aluminum obtained under various gravity fields at $T = 973$ K (700 °C), $t = 2$ min: (*a*) parallel sample, (*b*) upper residue at $G = 50$, (*c*) filtered aluminum at $G = 50$, (*d*) upper residue at $G = 100$, (*e*) filtered aluminum at $G = 100$, (*f*) upper residue at $G = 200$, (*g*) filtered aluminum at $G = 200$, (*h*) upper residue at $G = 500$, and (*i*) filtered aluminum at $G = 500$.

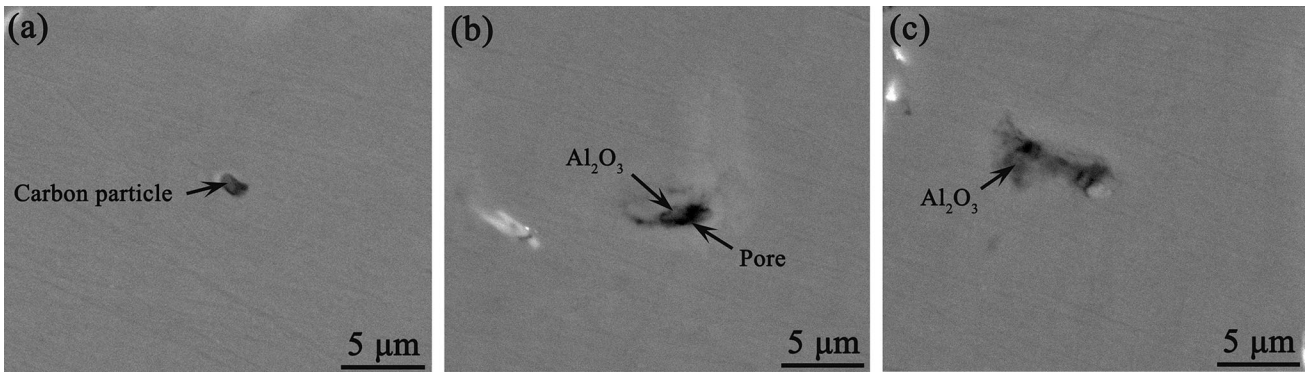

Fig. 10—Observation of fine inclusions in the filtered aluminum: (*a*) carbon particle, (*b*) granulous Al_2O_3 inclusion, and (*c*) filmy Al_2O_3 inclusion.

Table III. Variations of O and Titanium Contents in Samples and Removal Efficiency of Inclusions Obtained with Different Gravity Coefficients at t = 2 min and T = 973 K (700 °C)

Gravity Coefficient	O Content (mass pct)	Ti Content (mass pct)	Removal Efficiency of Inclusions (pct)	
			Oxide Inclusions	Al_3Ti
G = 1	0.4100	2.174	0.00	0.00
G = 50	0.0030	0.160	99.27	92.64
G = 100	0.0036	0.176	99.12	91.90
G = 200	0.0042	0.206	98.98	90.52
G = 500	0.0032	0.172	99.22	92.09
G = 600	0.0038	0.142	99.07	93.47

Table IV. Variations of O and Ti Contents in Samples and Removal Efficiency of Inclusions Obtained with Different Filtering Times at G = 50 and T = 973 K (700 °C)

Filtering Time (s)	O Content (mass pct)	Ti Content (mass pct)	Removal Efficiency of Inclusions (pct)	
			Oxide Inclusions	Al_3Ti
t = 0	0.4100	2.174	0.00	0.00
t = 15	0.0082	0.162	98.00	92.55
t = 30	0.0046	0.157	98.88	92.78
t = 60	0.0110	0.182	97.32	91.63
t = 120	0.0080	0.160	98.05	92.64
t = 300	0.0092	0.175	97.76	91.95

Table V. Variations of O and Ti Contents in Samples and Removal Efficiency of Inclusions Obtained with Different Filtering Temperatures at G = 50 and t = 2 min

Filtering Temperature, K (°C)	Oxygen Content (mass pct)	Ti content (mass pct)	Removal Efficiency of Inclusions (pct)	
			Oxide Inclusions	Al_3Ti
T = 933 (660)	0.0120	0.075	97.07	96.55
T = 973 (700)	0.0080	0.160	98.05	92.64
T = 1023 (750)	0.0060	0.311	98.54	85.69
T = 1073 (800)	0.0044	0.458	98.93	78.93

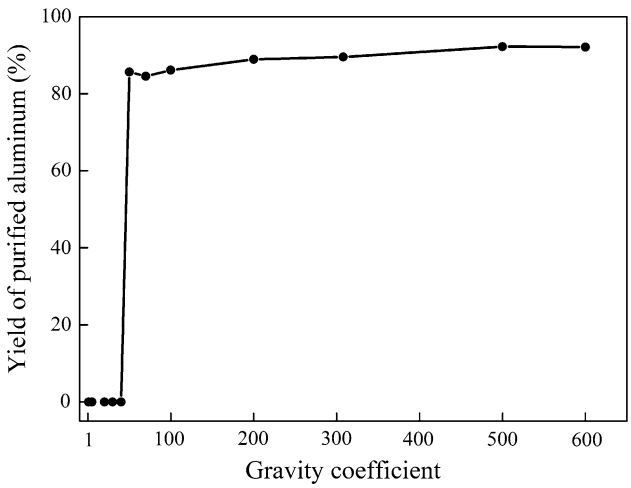

Fig. 11—Yield of purified aluminum obtained by filtration with different gravity coefficients at t = 2 min and T = 973 K (700 °C).

shown in Table III, indicating significant filtration efficiency. It also can be seen from Table IV that removal efficiencies of oxide inclusions and Al_3Ti particles can reach around 98 and 91 pct, respectively, at the filtering time $t \geq 15$ seconds. However, there is no clear relationship between the removal efficiency of inclusions and the gravity coefficient or filtering time when $G \geq 50$ or $t \geq 15$ seconds. Moreover, as shown in Table V, the removal efficiency of oxide inclusions increases slightly with increasing the filtering temperature, while the removal efficiency of Al_3Ti particles obviously decreases. When the filtering temperature is low, the viscous liquid aluminum tends to carry some inclusions (especially fine oxide inclusions) due to the large adhesive force during its flowing through the filter. It is well known that the solubility of Ti element in the aluminum melt increases with the increase of melt temperature, and the melt with more dissolved Ti will flow through the filter at a higher filtering temperature.

As can be seen from Tables III through V, the level of inclusion content in the filtered aluminum is reduced dramatically after supergravity filtration, and the filtered aluminum is called purified aluminum. The yield of purified aluminum is calculated as the ratio of the weight of filtered aluminum to the weight of the aluminum alloy before filtration. Figure 11 shows the yield of purified aluminum with different gravity coefficients at $t = 2$ minutes, $T = 973$ K (700 °C). Figure 12 presents the yield of purified aluminum with different filtering times at $G = 50$, $T = 973$ K (700 °C). Figure 13 shows the yield of purified aluminum with different filtering temperatures at $G = 50$, $t = 2$ minutes. As shown in Figure 11, the yield of purified aluminum obtained by filtration increases slightly with the increase of the gravity coefficient when $G \geq 50$. The yield of purified aluminum is up to 92.1 pct at $G = 600$, $t = 2$ minutes, and $T = 973$ K (700 °C). Besides, the yield of purified aluminum exceeds 80 pct within a short filtering time of 15 seconds, indicating that the supergravity filtration has an advantage of high efficiency for removing inclusions from molten melt. As illustrated in Figure 13, the yield of purified aluminum increases sharply with increasing the filtering temperature and the yield of purified aluminum increases quite slowly when the temperature $T \geq 973$ K (700 °C), which means that increasing the filtering temperature is beneficial to obtaining a great yield of purified aluminum. However, the removal efficiency of Al_3Ti reduces obviously with an increase in the filtering temperature. Moreover, molten aluminum is highly susceptible to absorption of hydrogen gas in high melt temperature, and the dissolved hydrogen tends to cause porosities in aluminum-based alloys during the rapid solidification process.[21] As shown in Figure 14(c), there are many large hole defects in the filtered aluminum obtained at $T = 1073$ K (800 °C). Therefore, the filtering temperature $T = 973$ K (700 °C) is the optimal for purifying the aluminum melt, considering the removal efficiency of inclusions and yield of purified aluminum.

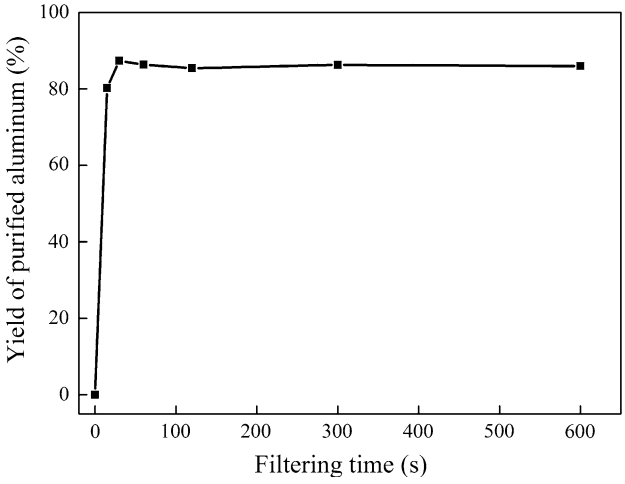

Fig. 12—Yield of purified aluminum obtained by filtration with different filtering times at $G = 50$ and $T = 973$ K (700 °C).

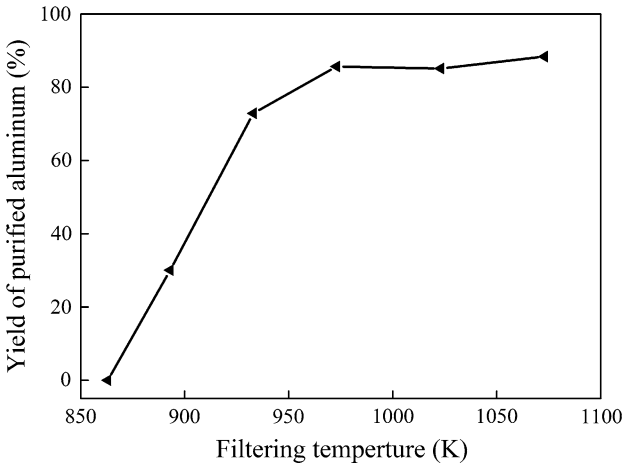

Fig. 13—Yield of purified aluminum obtained by filtration with different filtering temperatures at $G = 50$ and $t = 2$ min.

D. *Pressure Imposed on the Melt near the Filter under Various Gravity Fields*

A necessary consideration for removing inclusions from melts through filtration is the pressure drop (Δp) across the filter-molten metal interface, which is represented by the following Young–Laplace equation:[1]

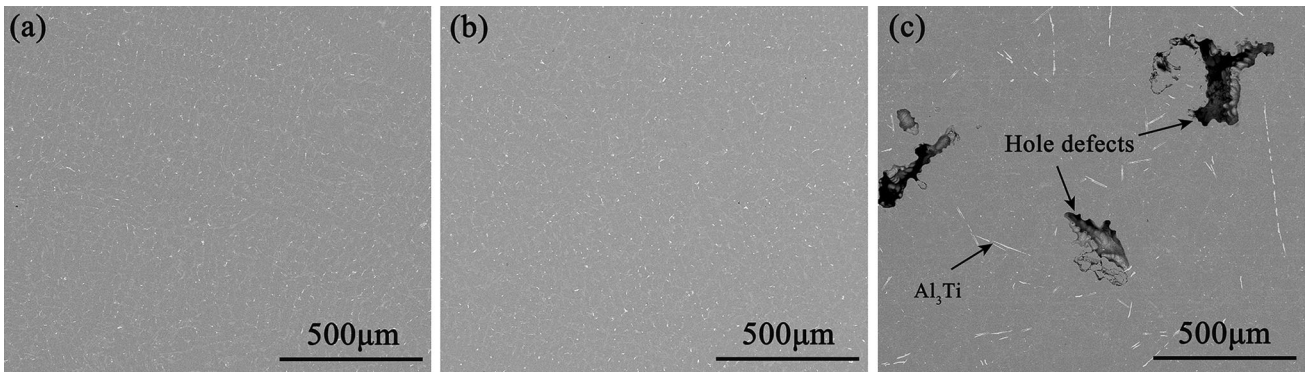

Fig. 14—Micrographs of the filtered aluminum obtained with different filtering temperatures: (*a*) $T = 933$ K (660 °C), (*b*) $T = 973$ K (700 °C), and (*c*) $T = 1073$ K (800 °C).

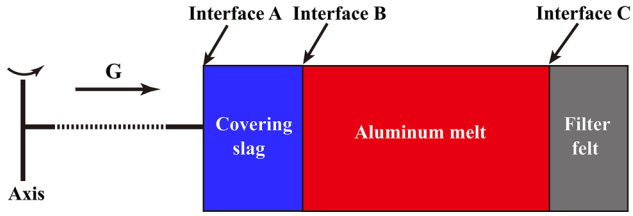

Fig. 15—Schematic drawing of phase interfaces for pressure calculation.

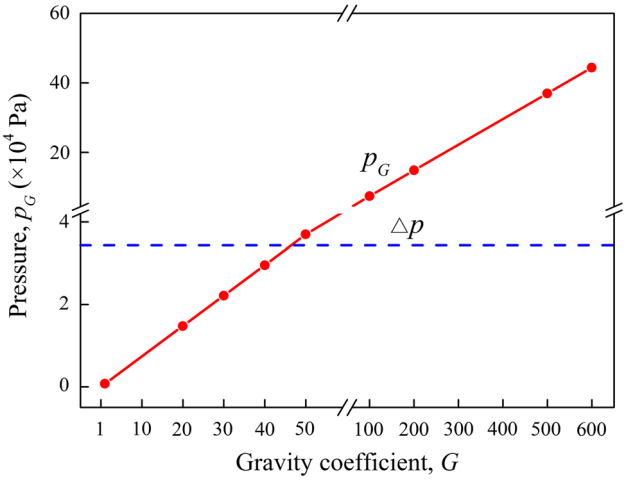

Fig. 16—Pressure generated on interface C with different gravity coefficients.

$$\Delta p = -\frac{4\sigma\cos\theta}{d} \quad [4]$$

where σ is the surface tension of molten aluminum, θ is the contact angle, and d is the average pore size of the filter felt. Substituting σ = 0.640 N/m,[22] θ = 127 deg,[23] and d = 44.78 μm into Eq. [4], Δp = 3.44 × 10^4 Pa, indicating that an external pressure (more than 3.44 × 10^4 Pa) is needed to get the melt to flow through the filter medium.

Under normal-gravity field, the pressure (p_g) imposed on the melt near the filter is given by the following equation:

$$p_g = \rho_m g h_m + \rho_c g h_c \quad [5]$$

where p_m is the density of aluminum melt, h_m is the height of aluminum melt, p_c is the density of covering slag, and h_c is the height of covering slag.

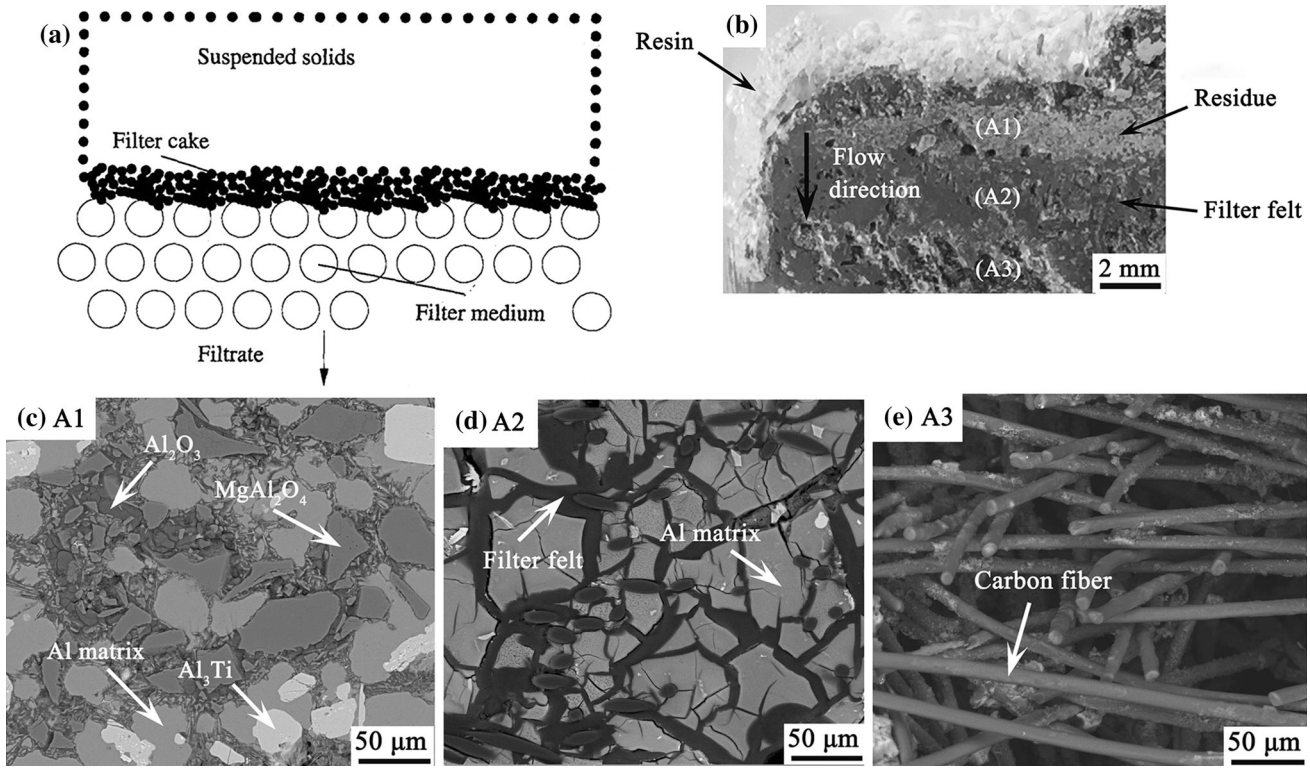

Fig. 17—Macrograph and micrographs of the filter felt and upper residue obtained by supergravity filtration: (*a*) schematic illustration of filter medium and cake, reprinted with permission from Ref. 27; (*b*) macrograph of the filter felt and residue; and (*c*), (*d*), and (*e*) micrographs of the areas marked with A1, A2, and A3 in (b), respectively.

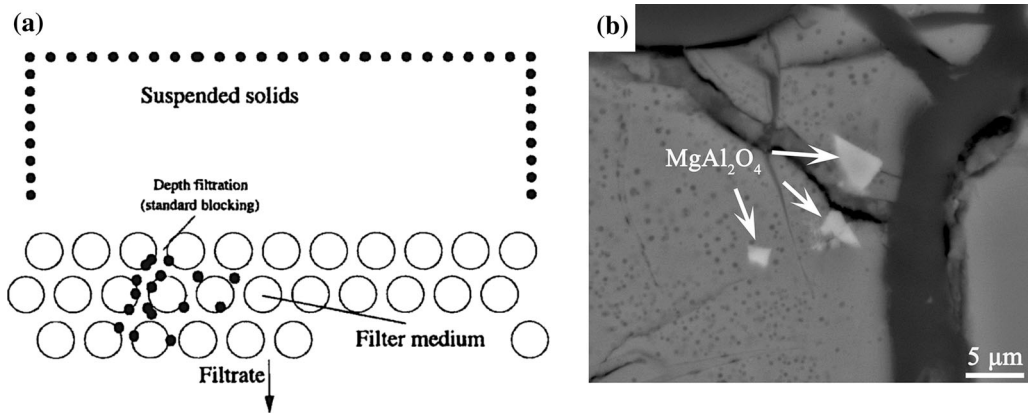

Fig. 18—Depth filtration phenomenon observed in the filter felt: (*a*) schematic diagram of depth filtration mode, reprinted with permission from Ref. 27; and (*b*) example of depth filtration observed in the filter felt.

Substituting $p_m = 2.685 \times 10^3$ kg/m^3,[18] $p_c = 1.875 \times 10^3$ kg/m^3, $h_m = 2.10 \times 10^{-2}$ m, $h_c = 1.00 \times 10^{-2}$ m, and g = 9.81 m/s^2 into Eq. [5], $p_g = 7.37 \times 10^2$ Pa. It is indicated that the pressure (p_g) hardly overcomes the pressure drop (Δp) to initiate the flow of the melt through the filter medium.

The centrifugal pressure (p_i) at the point i inside the melt is calculated *via* the following equation:[24]

$$p_i = \frac{\rho\omega^2\left(r_i^2 - r_0^2\right)}{2} \quad [6]$$

where ρ is the density of the melt, ω is the angular velocity, r_0 is the distance from the free liquid surface to the centrifugal axis, and r_i is the distance from point i to the centrifugal axis.

As illustrated in Figure 15, the pressure (p_G) generated on the interface C between the aluminum melt and filter medium can be written as

$$p_G = \frac{\rho_m\omega^2\left(r_c^2 - r_b^2\right)}{2} + \frac{\rho_c\omega^2\left(r_b^2 - r_a^2\right)}{2} \quad [7]$$

where r_c, r_b, and r_a are the distances from interfaces C, B, and A to the centrifugal axis, respectively.

Substituting $p_m = 2.685 \times 10^3$ kg/m^2, $p_c = 1.875 \times 10^3$ kg/m^3, $r_c = 0265$ m, $r_b = 0.244$ m, and $r_c = 0.234$ m into Eq. [7], and combining with Eq. [1], the centrifugal pressure is also expressed as

$$p_G = 7.39 \times 10^2\sqrt{G^2 - 1} \quad [8]$$

As shown in Figure 16, the pressure on the interface C increases almost linearly with an increase in the gravity coefficient. When the gravity coefficient $G < 50$, the pressure (p_G) is less than the pressure drop (Δp), and the molten melt hardly flows through the filter felt. The melt begins flowing to the lower container through the filter medium and the filtered aluminum is obtained at $G \geq 50$, because the pressure (p_G) can overcome the resistance from the filter felt, which agrees well with the experimental results, as shown in Figure 6. Therefore, supergravity filtration can well solve the problem of pressure drop (Δp) without meeting the rigorous requirement of height of molten metal, especially when using the fine-pore filter medium.

E. *Mechanism of the Supergravity Filtration with Carbon Felt Filter*

Generally, filters for separating solid particles from the liquid mainly operate in two mechanisms: cake-mode and deep-mode filtrations.[24] Further, these mechanisms for filtering the molten metal with CFFs have been investigated extensively.[25,26] However, it is necessary to investigate the filtration mechanism for the carbon felt filter used in this study. The residue-forming filter cake on the top of the filter felt is observed in Figure 17(b). A large number of oxide inclusions and Al_3Ti particles were gathered effectively in the residue obtained by supergravity filtration, as shown in Figure 17(c). During the filtration process, large inclusions are trapped on the top surface of the filter felt with fine porosity, while the aluminum melt can flow through the filter medium rapidly. Simultaneously, the filter cake formed with agglomerative inclusions can reduce the pore size of the filter felt and serve as another filter to intercept the smaller inclusions. This typical filtration mechanism is named cake-mode filtration and is illustrated in Figure 17(a). In deep-mode filtration, a small number of fine inclusions, especially oxide inclusions, are forced into the filter medium together with liquid aluminum under supergravity field. These fine inclusions are mechanically blocked by the crisscross carbon fibers, and the intricate structure of carbon fibers makes the long and winding route for inclusions to pass through the filter medium, as shown in Figures 17(d) and (e). Figure 18(a) schematically shows the typical depth filtration mechanism inside the filter medium, and a representative example of depth filtration is well observed in Figure 18(b). Although cake-mode and deep-mode filtrations are both observed as the filtration mechanism in the supergravity filtration experiments, cake-mode filtration is the major one.

IV. CONCLUSIONS

Separating inclusions from the molten aluminum by supergravity filtration with different gravity coefficients, various filtering times, and different filtering temperatures is investigated. Besides the positive pressure

generated by supergravity being calculated, the mechanism of supergravity filtration of aluminum melt is also discussed. The conclusions are summarized as follows.

1. Supergravity filtration is proven to be a promising method for removing inclusions from aluminum melt. The alloy samples can be divided automatically into two parts: the upper residue and the lower filtered aluminum. Further, all inclusions are almost intercepted in the upper residue by filter felt.
2. The removal efficiencies of oxide inclusions and Al_3Ti particles exceed 97.32 and 90.52 pct, respectively, at $G \geq 50$, $t \geq 15$ seconds, and $T = 973$ K (700 °C). The yield of purified aluminum obtained by filtration increases slightly with the increase of the gravity coefficient. The yield of purified aluminum is up to 92.1 pct at $G = 600$, $t = 2$ minutes, and $T = 973$ K (700 °C).
3. The removal efficiency of oxide inclusions increases slightly with an increase in the filtering temperature, while the removal efficiency of Al_3Ti particles sharply decreases. Although increasing the filtering temperature is beneficial to obtaining the great yield of filtered aluminum, many large defects are observed in the filtered aluminum.
4. The melt begins flowing to the lower container through the filter medium, and the filtered aluminum is obtained at $G \geq 50$, due to the fact that the pressure (p_G) generated by supergravity can overcome the resistance from the filter felt.
5. The filtration mechanisms of cake mode and deep mode are both observed in the upper residue and filter felt, but cake-mode filtration plays the major role.

ACKNOWLEDGMENTS

This work is financially supported by the National Natural Science Foundation of China (Grant Nos. 51234001 and 51274269). The authors are grateful to the State Key Laboratory of Advanced Metallurgy (University of Science and Technology Beijing) for the use of their supergravity apparatus. Sincere gratitude is also due to Professor Zhancheng Guo and Zhenya Zhang for their help and support.

REFERENCES

1. L.N.W. Damoah and L.F. Zhang: *Metall. Mater. Trans. B*, 2010, vol. 41B, pp. 886–907.
2. D. Shu, T.X. Li, B.D. Sun, Y.H. Zhou, J. Wang, and Z.M. Xu: *Metall. Mater. Trans. B*, 2000, vol. 31B, pp. 1527–33.
3. Y.J. He, Q.L. Li, and W. Liu: *Metall. Mater. Trans. B*, 2012, vol. 43B, pp. 1149–55.
4. Y.J. He, Q.L. Li, and W. Liu: *Mater. Lett.*, 2011, vol. 65, pp. 1226–28.
5. M.W. Kennedy, S. Akhtar, J.A. Bakken, and R.E. Aune: *Metall. Mater. Trans. B*, 2013, vol. 44B, pp. 691–705.
6. K. Li, J. Wang, D. Shu, T.X. Li, B.D. Sun, and Y.H. Zhou: *Mater. Lett.*, 2002, vol. 56, pp. 215–20.
7. M.W. Kennedy, S. Akhtar, J.A. Bakken, and R.E. Aune: *Light Metals*, John Wiley & Sons, Inc., San Diego, CA, 2011, pp. 763–68.
8. L.F. Zhang, S.Q. Wang, A.P. Dong, J.W. Gao, and L.N.W. Damoah: *Metall. Mater. Trans. B*, 2014, vol. 45B, pp. 2153–85.
9. G. Gaustad, E. Olivetti, and R. Kirchain: *Resources Conserv. Recycl.*, 2012, vol. 58, pp. 79–87.
10. K. Takahashi and S. Taniguchi: *ISIJ Int.*, 2003, vol. 43, pp. 820–27.
11. H. Zhao, L. Shao, and J.F. Chen: *Chem. Eng. J.*, 2010, vol. 156, pp. 588–93.
12. L.X. Zhao, Z.C. Guo, Z. Wang, and M.Y. Wang: *Metall. Mater. Trans. B*, 2010, vol. 41B, pp. 505–08.
13. S.W. Kim, U.H. Im, H.C. Cha, S.H. Kim, J.E. Jang, and K.Y. Kim: *China Foundry*, 2013, vol. 10, pp. 112–17.
14. J.W. Li, Z.C. Guo, H.Q. Tang, Z. Wang, and S.T. Sun: *Trans. Nonferrous Met. Soc. China*, 2012, vol. 22, pp. 958–63.
15. J.C. Li, Z.C. Guo, and J.T. Gao: *ISIJ Int.*, 2014, vol. 54, pp. 743–49.
16. J.C. Li and Z.C. Guo: *Metall. Mater. Trans. B*, 2014, vol. 45B, pp. 1272–80.
17. J.C. Li, Z.C. Guo, and J.T. Gao: *Ironmaking and Steelmaking*, 2014, vol. 41, pp. 776–83.
18. G.Y. Song, B. Song, Y.H. Yang, Z.B. Yang, and W.B. Xin: *Metall. Mater. Trans. B*, 2015, vol. 45B, pp. 2190–97.
19. R. Fritzsch, M.W. Kennedy, J.A. Bakken, and R.E. Aune: *Light Metals*, TMS, Hoboken, NJ, 2013.
20. M. Jaradeh and T. Carlberg: *Mater. Sci. Eng. A*, 2005, vols. 413–414, pp. 277–82.
21. J.P. Harvey and P. Chartrand: *Metall. Mater. Trans. B*, 2010, vol. 41B, pp. 908–24.
22. D. Emadi, J.E. Gruzleski, and J.M. Toguri: *Metall. Trans. B*, 1993, vol. 24B, pp. 1055–63.
23. H. Uozumi, K. Kobayashi, K. Nakanishi, T. Matsunaga, K. Shinozaki, H. Sakamoto, T. Tsukada, C. Masuda, and M. Yoshida: *Mater. Sci. Eng. A*, 2008, vol. A495, pp. 282–87.
24. J.P. Nielson: *J. Dent. Res.*, 1978, vol. 57, pp. 261–69.
25. M. W. Kennedy: Ph.D. Thesis, Norwegian University of Science and Technology, Trondheim, 2013.
26. X. Cao: *Metall. Mater. Trans. B*, 2006, vol. 37B, pp. 1075–83.
27. A. Rushton, A.S. Ward, and R.G. Holdich: *Solid-Liquid Filtration and Separation Technology*, 2nd ed., Wiley-VCH, New York, NY, 2000.